On-site interband excitations in resonant inelastic x-ray scattering from Cu_2O

J. P. Hu, D. J. Payne, and R. G. Egdell*
Department of Chemistry, Inorganic Chemistry Laboratory, South Parks Road, Oxford OX1 3QR, United Kingdom

P.-A. Glans, T. Learmonth, and K. E. Smith
Department of Physics, Boston University, 590 Commonwealth Avenue, Boston, Massachusetts 02215, USA

J. Guo
Advanced Light Source, Lawrence Berkeley National Laboratory, Berkeley, California 94720, USA

N. M. Harrison
STFC, Daresbury Laboratory, Warrington, Cheshire, WA4 4AD, United Kingdom
and Department of Chemistry, Imperial College, London, SW7 2AZ, United Kingdom
(Received 8 January 2008; revised manuscript received 5 March 2008; published 15 April 2008)

The electronic structure of cuprite (Cu_2O) has been studied by high-resolution x-ray photoemission (XPS), x-ray absorption (XAS), and resonant x-ray emission spectroscopies (XES) supported by band structure calculations using a hybrid exchange approximation to density functional theory. A pronounced loss feature at about 4.5 eV due to on-site interband excitation has been identified in resonant inelastic x-ray scattering from Cu_2O close to the L_3 (Cu $2p_{3/2}$) core threshold. Although Cu_2O nominally has a filled upper valence band of Cu $3d$ states and an empty conduction band of Cu $4s$ states, the band structure calculations show that there is substantial $3d$ character in the conduction band and that the inelastic loss is dominated by on-site $3d$ to $3d$ excitation conforming to the selection rule $\Delta l=0$ rather than $3d$ to $4s$ transitions with $\Delta l=-2$. However, unlike in previous work, these transitions do not arise from ligand field splitting of the Cu $3d$ states but rather from on-site $3d$-$4s$ hybridization which introduces $3d$ character into the conduction band. Comparison between XPS, XES, and XAS data shows that Cu L_3 XAS is dominated by a core exciton lying 0.65 eV below the bottom of the conduction band and that inelastic scattering is only observed for photon energies below that required to excite the core electron into the conduction band.

DOI: 10.1103/PhysRevB.77.155115 PACS number(s): 73.20.At, 73.43.Cd, 78.70.En

I. INTRODUCTION

There is a growing interest in the development of electronic and optoelectronic devices based on oxides which are transparent in the visible region but which can be doped to induce a high electrical conductivity. Most of the established transparent conducting oxides (TCOs) of this sort are n-type materials.[1] This includes the prototype TCOs SnO_2, In_2O_3, and ZnO. It has been proven to be very difficult to develop reproducible strategies for the p-type doping of these materials.[2–4] However, exploitation of transparent conducting oxides in devices such as UV diodes will only become possible if suitable wide gap oxides that can be doped p-type can be developed. In the classical n-type TCOs, the top of the valence band is composed of O $2p$ states and it is not surprising that it is difficult to introduce holes into these bands: in chemical terms, one is attempting to oxidize oxygen. However, in cuprite (Cu_2O), the upper valence band states are of dominant Cu $3d$ atomic character and introduction of holes involves oxidation of $3d^{10}$ Cu(I) to $3d^9$ Cu(II). This process is chemically tractable and Cu_2O is indeed a p-type semiconductor. The electronic band gap in Cu_2O is 2.17 eV (Ref. 5) and is therefore too small for the application in TCO devices. However, the band gaps in many ternary Cu(I) oxides are much bigger than in the parent Cu_2O. This has allowed development of new families of p-type conducting ternary Cu(I) oxides that are transparent in the visible region.[6–13] Cu_2O itself has emerged as a p-type host for doping with magnetic ions in order to induce room temperature dilute semiconductor ferromagnetism.[14–17] The recent interest in the functional properties of Cu(I) oxides has prompted us to revisit the electronic structure of Cu_2O. The main focus of the present paper is the investigation of the nature of electronic excitations in Cu_2O found in resonant inelastic x-ray scattering (RIXS) at the Cu L_3 edge. Previous photon excited x-ray emission spectroscopy (XES) studies of Cu_2O have been restricted to the Cu K (Refs. 18 and 19) and Cu $M_{3,2}$ (Ref. 20) edges. In both cases, resolution was limited by very pronounced lifetime broadening (>1.5 eV) of the core hole and no attempt was made to study resonant x-ray scattering. Elsewhere, electron beam excited Cu L and O K emission spectra were reported many years ago,[21] but again with poor overall effective resolution and with no possibility to study resonant emission. The discovery of pronounced resonant inelastic x-ray scattering at the Cu L_3 edge in the current study prompted reexamination of high-resolution x-ray photoemission spectroscopy (XPS) and x-ray absorption spectroscopy (XAS) spectra of Cu_2O. In contrast to previous valence region XPS studies,[22,23] particular care was taken to establish the position of the Fermi level relative to the valence band edge. This then enabled exploration of the relationship between core level binding energies in XPS and the energies of features in XAS and XES. It is shown that the Cu L_3 absorption spectrum[24–26] is dominated by a core-hole exciton that lies 0.65 eV below the bottom of the conduction band. The experimental work is supported by band structure calcula-

tions using a hybrid exchange approximation to density functional theory that gives an accurate first principles description of the bulk band gap. The combined experimental and theoretical study leads to the identification of a general mechanism for inelastic x-ray scattering in Cu(I) compounds.

The primitive cubic structure of Cu_2O belongs to the space group O_h^4 and is based on a body centered cubic array of oxygen ions with Cu ions occupying half the sites between adjacent oxygen ions. The O ions are found at (0,0,0) and (1/2,1/2,1/2) and the Cu ions at (1/4,1/4,1/4), (3/4,1/4,3/4), (1/4,3/4,3/4), and (3/4,3/4,1/4), giving two formula units per cell. The structure can alternatively be described in terms of two interpenetrating anti-SiO_2 cristabolite nets.[27] In this structure, the Cu ions occupy sites with linear coordination by two O ions, although due to a staggered arrangement of the three additional Cu ions bonded to these two oxygen ions, the local site symmetry is D_{3d}. In addition, the separation between adjacent Cu ions in the two different nets is quite small (~3.02 Å) allowing significant interaction between them. This, in turn, influences the width of the valence band. The O ions are surrounded by four copper ions in a tetrahedral arrangement. The unusual structure is associated with negative thermal expansion.[28]

In the simplest ionic model description, Cu_2O is a d^{10} oxide. An upper valence band of filled Cu $3d$ states sits above a band of filled O $2p$ states, while the bottom of the conduction band is nominally composed of Cu $4s$ states with empty Cu $4p$ states at higher energy. In terms of the linear O-Cu-O units, the Cu $3d_{z^2}$ orbitals have σ-like symmetry, the $3d_{xz}$ and $3d_{yz}$ orbitals have π-like symmetry, and the $3d_{xy}$ and $3d_{x^2-y^2}$ orbitals have δ-like symmetry. Thus, O $2p$ orbitals can mix with Cu $3d_{z^2}$ via strong σ overlap and with $3d_{xz}$ and $3d_{yz}$ via weaker π interactions. However, the $3d_{xy}$ and $3d_{x^2-y^2}$ orbitals must remain localized on Cu as there are no orbitals on oxygen of the correct δ symmetry for covalent mixing. Within this description, the lowest energy interband transitions of Cu_2O are basically from a filled upper valence band of Cu $3d$ states (mixed to some extent with O $2p$ states) into an empty conduction band of Cu $4s$ states. Interband excitations are therefore on-site transitions conforming to a change in angular momentum $\Delta l=-2$, which makes the transitions allowed in inelastic x-ray Raman scattering where the atomic selection rule is $\Delta l=0,\pm 2$. However, the band calculations show that due to extensive mutual mixing between O $2p$, Cu $3d$, and Cu $4s$ states, this simple description must be modified. It transpires that on-site $4s$-$3d$ hybridization introduces significant Cu $3d$ character into the conduction band so that even though Cu_2O is nominally a $3d^{10}$ oxide, the interband transitions have significant $3d$ to $3d$ character and thus satisfy $\Delta l=0$. This allowed channel is mediated exclusively by matrix elements between core Cu $2p$ states and Cu $3d$ states and does not involve matrix elements between Cu $2p$ and Cu $4s$ states. Since the former are much bigger,[26,29] the energy loss is dominated by the full and empty Cu $3d$ partial densities of states.

II. ELECTRONIC STRUCTURE CALCULATIONS

The calculations presented have been performed using the CRYSTAL06 software.[30] Electronic exchange and correlation were approximated using the hybrid exchange formalism which has previously been demonstrated to provide a reliable description of the ground state electronic structure in copper oxides[31] and, of particular relevance to the current study, of the nature and value of the band gap in a wide variety of materials.[32] The most significant numerical approximation is the expansion of the crystalline orbitals in a basis set consisting of a linear combination of atom centered Gaussian orbitals. High quality all-electron basis sets used in previous studies[33,34] were adopted to describe the Cu and O ions and the outermost exponents re-optimized *in situ*. This resulted in the use of a quadruple valence set for the Cu ion of structure 864111-D31 with outer sp exponents (in a_0^{-2}) of 1.582, 0.559, and 0.15 and outer d exponent of 0.430. The triple valence O basis set, 8411D, had outer sp exponents of 0.425 and 0.125 with a d exponent of 0.5. The Coulomb and exchange series were truncated using overlap criteria documented elsewhere[30] (strict tolerances of 7 7 7 7 14 were adopted) and the exchange correlation potentials and energy were integrated numerically on an atom centered grid of points containing approximated 2500 symmetry irreducible points per atom (the XLGRID option[30]). Finally, k-space integration was performed on a Pack–Monkhurst grid defined by a shrinking factor of 8 which contained 59 symmetry irreducible points.

III. EXPERIMENT

Cu_2O was prepared by decomposing CuO under flowing Ar at 900 °C. The high purity powder sample was pressed into disks between tungsten carbide dies and further sintered under Ar at 900 °C to give robust ceramic disks. Phase purity was confirmed by x-ray powder diffraction.

High-resolution x-ray photoemission spectra were measured in a Scienta ESCA 300 spectrometer. This incorporates a rotating anode Al $K\alpha$ ($h\nu$=1486.6 eV) x-ray source, a seven crystal x-ray monochromator, and a 300 mm mean radius spherical sector electron energy analyzer with parallel electron detection system. The x-ray source was run with 200 mA emission current and 14 kV anode bias, while the analyzer operated at 150 eV pass energy with 0.8 mm slits. The Gaussian convolution of the analyzer resolution with a linewidth of 260 meV for the x-ray source gives an effective instrument resolution of 350 meV. Spectra were measured in normal emission. The Cu_2O sample was cleaned by a surface science recipe which involved bombardment with Ar ions, followed by annealing in order to heal ion beam damage.[35–37] Following bombardment with 2.5 kV Ar ions for 15 min followed by annealing in UHV (5×10^{-9} mbar) at first 550 °C and then 650 °C for 1 h, the O $1s$ core line assumed a narrow profile (full width at half maximum height of 0.66 eV) with a symmetric shape and a without high binding energy shoulder due to surface adsorbates. In addition, satellites due to CuO were eliminated from Cu $2p$ core level spectra. Finally, the Cu $2p$ to O $1s$ intensity ratio after correction for atomic sensitivity factors[38] assumed a value of 1.54, which is within the range found for ordered single crystal $Cu_2O(100)$ surfaces with Cu terminated reconstructions.[35,36] The C $1s$ to O $1s$ intensity ratio was reduced to below 1/100. Binding

energies are referenced to the Fermi energy of a silver sample regularly used to calibrate the spectrometer.

X-ray absorption and emission spectra were measured at beamline 7.0.1 at the Advanced Light Source, Lawrence Berkeley National Laboratory. This beamline is equipped with a spherical grating monochromator.[39] Emission spectra were recorded using a Nordgren-type grazing-incidence spherical grating spectrometer.[40] For resonant emission experiments, the beamline was set to have an energy resolution of 500 meV at the O K edge and 1 eV at the Cu L_3 edge, and the emission spectrometer was set to have a resolution of 350 meV for O K and 750 meV for Cu L_3 edge spectra. Absorption spectra were measured in total fluorescence yield and total electron yield modes. For the absorption measurements, the beamline resolution was set to 200 meV for the O K edge and to 1 eV for the Cu L_3 edge. The absorption spectra were normalized to a reference current from a clean gold mesh positioned in the path of the photon beam. The energy scale of the O K absorption spectra was calibrated relative to the O K absorption spectrum of NiO and the Cu L absorption spectra were calibrated relative to the L absorption spectrum of Cu metal. The O K-edge emission spectra were calibrated to Zn $L\alpha_{1,2}$ and $L\beta_1$ emission lines of Zn metal in second order, and the Cu L-edge emission spectra were calibrated relative to metallic Cu $L\alpha_{1,2}$ and $L\beta_1$ emission spectra measured in first order. All emission spectra were measured with the spectrometer set at 90° to the incoming photon beam, which was itself incident at 25° relative to the sample surface. The consistency of the calibrations in XPS and XES is demonstrated by the fact that the peak maximum in nonresonant Cu L_3 XES (corresponding to the position of the peak maximum in the Cu 3d partial density of states relative to the Cu $2p_{3/2}$ core hole) is at 929.4 ± 0.2 eV, while the separation between the Cu $2p_{3/2}$ core level and valence band peak maxima (the latter again corresponding to the position of the peak maximum in the Cu 3d partial density of states) in XPS is 929.5 ± 0.1 eV.

IV. RESULTS AND DISCUSSION

A. Electronic density of states

The full and partial densities of states derived from the band structure calculations are shown in Fig. 1. The occupied full and empty densities of states are in broad general agreement with the previous work[41–49] although with exception of the semiempirical calculations of Robertson[43] and the self-interaction corrected local density approximation (LDA) calculation of Filippetti and Fiorentini,[48] the present calculations reproduce the experimental band gap and valence bandwidth much better than previously (Table I). In particular, earlier density functional calculations[42,44,46] underestimated the bulk band gap, whereas a Hartree–Fock calculation[45] dramatically overestimated the gap. The failure of these well-established methods is well known and has been discussed in many previous publications.[32,50] The hybrid method used in the present work introduces an element of the Hartree–Fock exchange into the density functional Hamiltonian and has been shown to give accurate predictions of bulk band gaps for a very wide range of materials.[32]

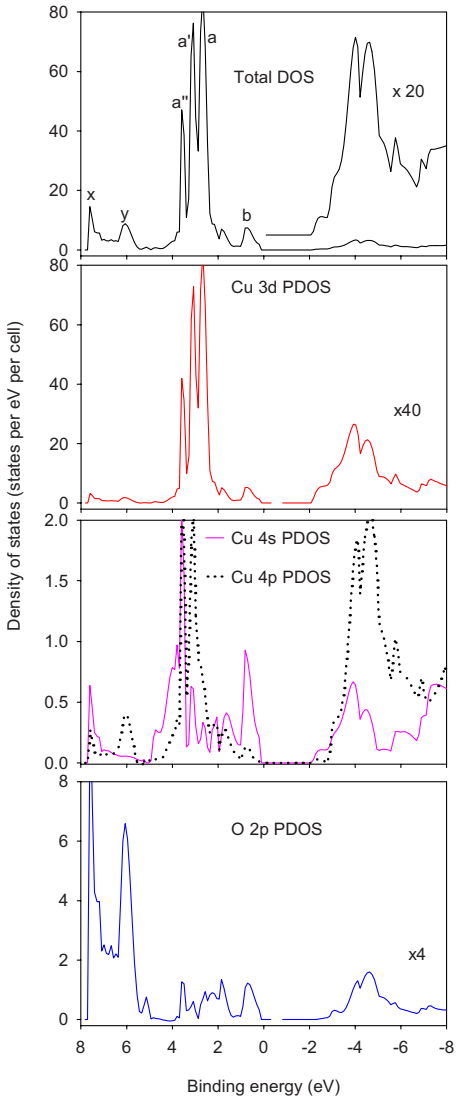

FIG. 1. (Color online) Full and partial densities of states for Cu_2O derived from band structure calculations.

Looking in more detail at the full and partial densities of states, it can be seen that the upper part of the valence band is of dominant Cu 3d atomic character and the lower part is of dominant O 2p character. The lower O 2p states are themselves split into two components x and y. There is significant covalent mixing of Cu 3d character into both x and y, although the Cu 3d contribution is slightly stronger in the more tightly component x: the Cu 3d/O 2p ratio at the maximum in x is 0.32, whereas the ratio at the maximum in y is 0.28. The structure in the Cu 3d part of the valence band contains a strong peak labeled a in Fig. 1, which has two subsidiary maxima a' and a'' on the high binding energy side, together with a weaker peak b at lower binding energy and close the top of the valence band. There is, in turn, covalent mixing of O 2p character into the Cu 3d states. It is, however, striking that this mixing is much stronger in b than in a. Thus, the O 2p/Cu 3d ratio at the peak maximum in b is 0.23, whereas the ratio at the peak maximum in a is 0.008. This accords with the qualitative discussion outlined in Introduction which led us to anticipate that states at the top of the valence band

TABLE I. Band gaps and valence bandwidth in Cu_2O from band structure calculations compared to experimental data.

Reference	Technique	Band gap (eV)	Valence bandwidth (eV)
42	Self-consistent LDA[a] with localized Gaussian basis and Slater exchange	1.1	6.0
43	Parameterized semiempirical tight binding	2.2	8.2
44	LAPW[b]	~0.6	6.8
45	Hartree–Fock with DFT[c] correction	9.7	7.0
46	GGA FP-LAPW[d] (WIEN97)	~0.5	7.2
47	LDA GP-LAPW	0.52	7.2
48	LDA	0.55	7.5
	LDA with SIC	1.80	8.2
49	DFT	~0.5	7.5
5	Experimental	2.17	
Present	Hybrid exchange DFT[c]	2.1	7.8
Present	Experimental		~8.0

[a]Local density approximation.
[b]Linear augmented plane wave.
[c]Density functional theory.
[d]Generalized gradient approximation full potential linear augmented plane wave.
[e]General potential linearized augmented plane wave.

should be antibonding and involve mixing between the σ-like Cu $3d_{z^2}$ orbitals and an appropriately symmetrized linear combination of σ-like O $2p$ orbitals. By contrast, the band *a* contains δ-like Cu $3d_{z^2-y^2}$ and Cu $3d_{xy}$ states which cannot mix with O $2p$ states, as well as the Cu $3d_{xz}$ and Cu $3d_{yz}$ states which can only mix with O $2p$ states via weak π-type overlap. These qualitative ideas are in agreement with the conclusions of Marksteiner *et al.*,[44] who performed a projection of the Cu $3d$ partial density of states into local σ, π, and δ components. This earlier work showed that σ-like Cu $3d_{z^2}$ character was found in band *b* and in band *x* at the top and bottom of the valence band, respectively. In addition, Marksteiner *et al.*[44] found that there was also a significant contribution from Cu $3d_{z^2}$ states at the bottom of band *a* in a'', which lies between the main O $2p$ and Cu $3d$ valence bands. Turning back to the discussion of our own calculations, we find that in contrast to the simple ionic model description which treats Cu^+ as a $3d^{10}4s^0$ cation, significant Cu $4s$ character is found in the valence band. Three pronounced maxima are found in the Cu $4s$ occupied partial density of states at energies corresponding to the peaks *b*, a'', and *x*. Two of these maxima (those in *b* and a'') in the Cu $4s$ partial density of states therefore coincide with the maxima in the Cu $3d$ partial density of states, indicating that there is pronounced on-site $3d$-$4s$ hybridization. This finding is in agreement with qualitative ideas first developed by Orgel[51] that rationalized the linear coordination found for Cu(I) compounds in terms of on-site Cu $3d$–Cu $4s$ mixing. These conclusions are also in accord with very recent LDA+U calculations and angle resolved photoemission measurements which found evidence for a state with mixed Cu $3d$ and Cu $4s$ character between the main band of Cu $3d$ states and the O $2p$ band.[52] The overall width of the Cu $3d$ part of the valence band in Cu_2O is found to be about 4.0 eV in our calculations. This is significantly greater than the value of 2.8 eV for $SrCu_2O_2$ found in a recent calculation using the same hybrid Hamiltonian approach adopted here.[53] This is despite the fact that the next neighbor coordination of Cu by two O ions in a linear arrangement in $SrCu_2O_2$ is similar to that in Cu_2O and the Cu-O bond lengths have almost identical values of 1.85 Å (Cu_2O) and 1.84 Å ($SrCu_2O_2$). The main difference between the two oxides is in the dimensionality of next-nearest neighbor interactions between the Cu $3d^{10}$ shells. In Cu_2O, each Cu ion has 12 next-nearest Cu neighbors (6 of which belong to the interpenetrating framework) in a three-dimensional arrangement with a Cu-Cu separation of 3.01 Å. In $SrCu_2O_2$, by contrast, there are only two next-nearest Cu neighbors in a linear two-dimensional arrangement, although with a reduced Cu-Cu separation of 2.74 Å. The smaller Cu $3d$ bandwidth in $SrCu_2O_2$ and the associated increase in the band gap reflect this difference.

Turning now to the empty density of states in Cu_2O, it can be seen in Fig. 1 that Cu $4s$ and Cu $3d$ states make the strongest contributions to the bottom of the conduction band. At higher energy, the Cu $4p$ contribution becomes dominant. In addition, there is a significant O $2p$ contribution to the conduction band.

B. X-ray photoemission and nonresonant x-ray emission spectra

Experimental valence band x-ray photoemission spectra of Cu_2O are shown in Fig. 2 along with O *K* and Cu L_3 x-ray emission spectra excited under nonresonant conditions well

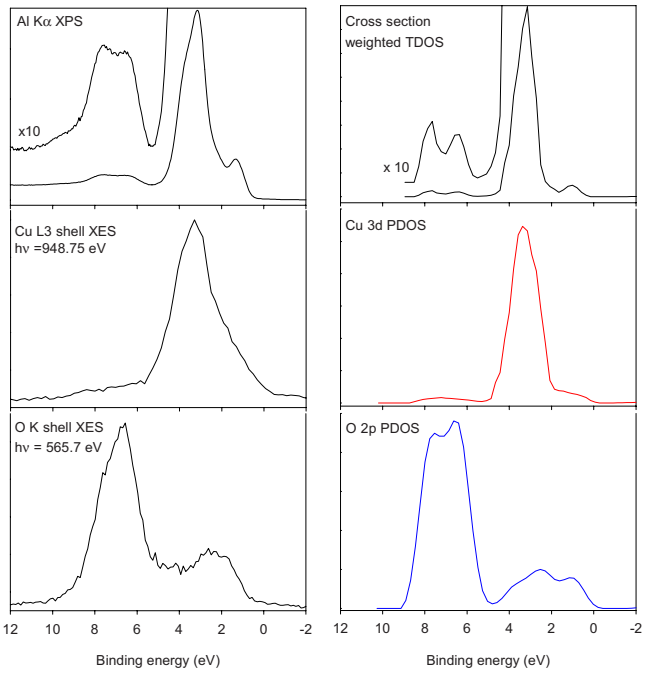

FIG. 2. (Color online) Left hand panels: Al $K\alpha$ excited valence band x-ray photoemission and nonresonant Cu L_3 and O K x-ray emission spectra of Cu_2O. Right hand panels: cross section weighted density of states and Cu $3d$ and O $2p$ partial densities of states for Cu_2O appropriately broadened.

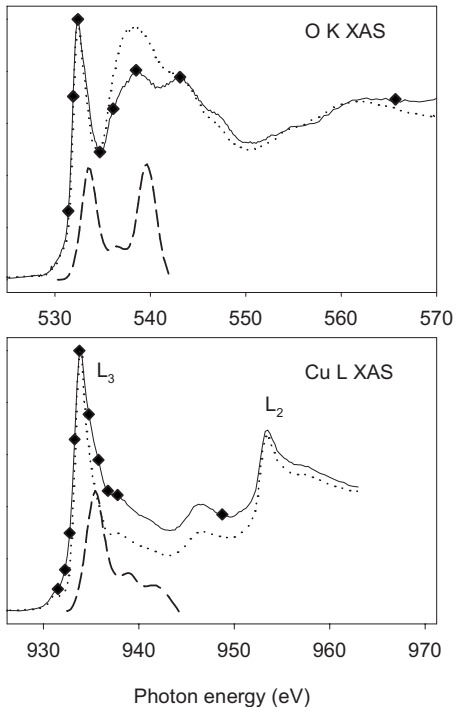

FIG. 3. Solid lines: x-ray absorption spectra for Cu_2O measured close to the O K and Cu L edges in the total fluorescence yield mode. Dotted line: as above but measured in total electron yield mode. Dashed lines: empty O $2p$ and Cu $3d$ partial densities of states from band structure calculations. The diamonds indicate the energies at which x-ray emission spectra were excited.

above the core threshold. The photoemission spectrum is compared to the density of states from the band structure calculations with the differing partial contributions to the total density of states weighted in proportion to one electron ionization cross section computed at $h\nu$=1486.6 eV. At this energy, the one electron cross section for ionization of Cu $3d$ states is a factor of 20 bigger than the cross section for ionization of O $2p$ states.[54] The overall cross section weighted density of states is therefore dominated by the Cu $3d$ partial density of states. The experimental spectrum is in agreement with the calculation both in terms of the overall shape of the spectral profiles and in terms of the relative intensities of the upper and lower parts of the valence band. In particular, much of the intensity in the O $2p$ region in the lower half of the valence band is a direct reflection of covalent mixing of Cu $3d$ character into the lower valence band states. However, there is a small but significant contribution to the intensity in this region from the O $2p$ states themselves. Conversely, the O K shell x-ray emission spectrum is a direct measure of the O $2p$ partial density of states. The lower valence band states are the strongest spectral features, but again due to covalency, there is significant intensity in the upper valence band region. In agreement with the calculations, there is, however, little intensity in the region of the most tightly bound Cu $3d$ states which dominate the x-ray photoemission spectrum. This reflects the fact that these states have local δ character and cannot therefore mix with O $2p$ states. Finally, the Cu L_3 emission spectrum is a probe of the Cu $3d$ partial density of states but without any O $2p$ contribution. The spectral profile is similar to the x-ray photoemission spectrum although with poorer resolution. However, it is noticeable that the lower valence band structure is slightly weaker relative to the Cu $3d$ maximum than in x-ray photoemission. This is because the O $2p$ partial density of states makes a small contribution to x-ray photoemission intensity but not to Cu L_2 x-ray emission.

C. X-ray absorption spectra and core lines in x-ray photoemission

O K and Cu $L_{2,3}$ x-ray absorption spectra are shown in Fig. 3. Both spectra contain a strong and relatively narrow peak close to the absorption threshold with maxima at 532.4 and 933.7(5) eV, respectively. These energies are in excellent agreement with the corresponding values of 933.7 and 532.5 eV found by Grioni *et al.*[25] The O K shell absorption spectrum basically mimics the unoccupied O $2p$ partial density of states. However, the strikingly asymmetric line shape in the threshold peak of the Cu L_3 spectrum is not reproduced by the band structure calculations. The spectrum can be regarded as a superposition of an excitonic component at threshold with structure at higher energy that is associated with the empty density of states.[25]

It is interesting to consider the energies of the absorption maxima above threshold in relation to the associated core level binding energies. The O $1s$ and Cu $2p_{3/2}$ XPS core level spectra are shown in Fig. 4. The full widths at half maximum heights for these core lines are 0.66 and 1.32 eV, respectively, very much lower than in previous work. The linewidths are, however, bigger than the resolution of the XPS

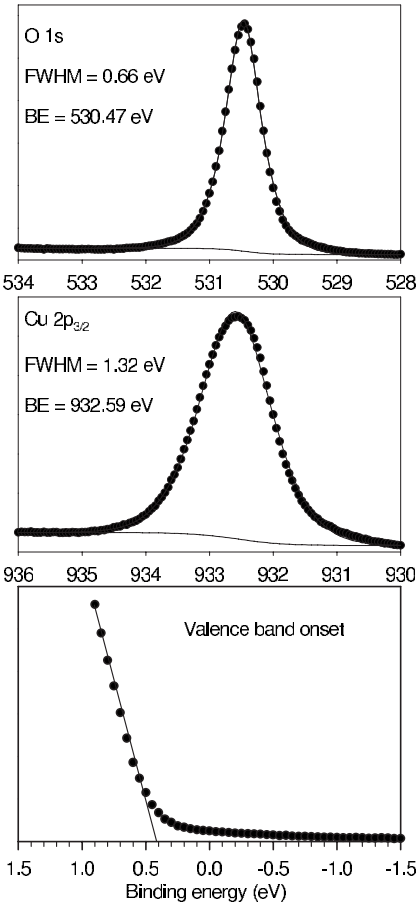

FIG. 4. O 1*s* and Cu $2p_{3/2}$ core Al $K\alpha$ photoemission spectra of Cu_2O. Binding energies are referenced to the Fermi level. The valence band onset spectrum in the bottom level shows that the Fermi level is found 0.4 eV above the valence band maximum.

system and probably represent the intrinsic linewidths determined by phonon and lifetime broadening. The O 1*s* binding energy is found to be 530.5 eV and the Cu $2p_{3/2}$ binding energy 932.6 eV. These binding energies are both in good agreement with previous work[23] and are referenced to the Fermi energy. As shown in the bottom panel of Fig. 4, the valence band edge in XPS is ~0.4 eV below the Fermi level. Given that the band gap is 2.2 eV (to the nearest 0.1 eV), the bottom of the conduction band is determined to be 2.2−0.4 eV=1.8 eV above the Fermi level. The maximal amplitudes in the computed empty O 2*p* and Cu 3*d* partial densities of states are, in turn, found in the band structure calculations of 2.2 and 1.7 eV, respectively, above the bottom of the conduction band. Thus, the peak maxima in the absorption spectra are expected at 530.5+1.8+2.2 eV =534.5 eV for the O *K* edge and at 932.6+1.8+1.7 eV =936.1 eV Cu L_3 edges. The actual maxima are found at 532.4 and 933.75 eV, representing downward shifts of 2.1 eV for the O *K* spectrum and 2.35 eV for the Cu L_3 spectrum. These energies are shown in Fig. 5. The shifts must be attributed to the effects of the core-hole potential as discussed earlier by Grioni *et al.*[25] The peak maximum in the Cu L_3 absorption spectrum lies 0.65 eV below the bottom of the conduction band (Fig. 5) and therefore corresponds to a

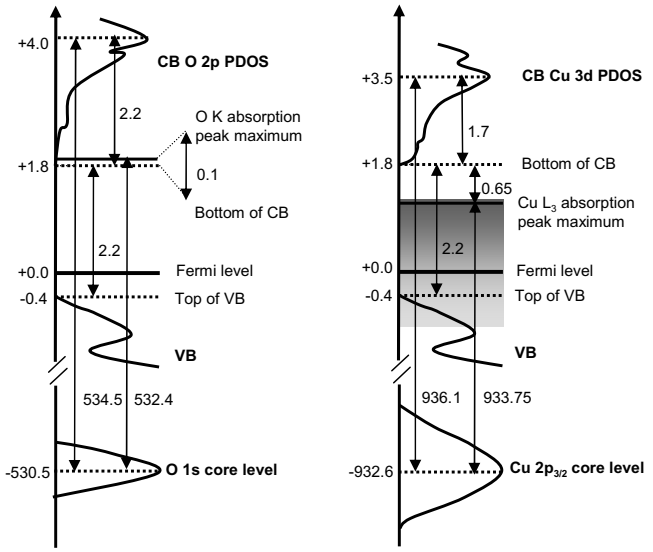

FIG. 5. Schematic energy level diagram showing the relationship between energies in XPS, XAS, and XES for O *K* and Cu L_3. The shaded region indicates the range of photon energies over which resonant inelastic scattering is observed at the Cu L_3 edge.

true split-off core-hole exciton. By contrast, the peak maximum in the O *K* absorption spectrum is 0.1 eV above the conduction band minimum and therefore corresponds to an excitonic resonance embedded in the conduction band.

D. Inelastic x-ray scattering

O *K* x-ray emission spectra of Cu_2O excited at the range of photon energies depicted in Fig. 3 are shown in Fig. 6. There is little change in the spectra with varying photon energy, and in all cases, the spectra seem to be dominated by the occupied O 2*p* partial density of states. By contrast, there is a clear variation in the energy of spectral emission structure with exciting photon energy in the range between $h\nu$ =931.50 eV and $h\nu$=933.75 eV for the Cu L_3 emission spectra shown in Fig. 7. When the spectra are transposed onto an energy loss scale, it is seen that a feature at a constant energy loss of 4.5 eV appears over the photon energy range 931.5eV$<h\nu<$933.75 eV. Above 933.75 eV, the spectra evolve toward the nonresonant spectrum previously discussed, with the appearance of distinct shoulders on both the low and high energy sides of the main peak.

The loss structure near to threshold is interpreted in terms of interband excitations in Cu_2O. Following Kotani and Shin[55] and Jiménez-Mier *et al.*,[56] the intensity of inelastically scattered photons at energy ω for incident energy Ω may be written in terms of filled and empty partial densities of states ρ_m and ρ_n,

$$F(\Omega,\omega) \propto \sum_{m,n} |\langle \phi_{\mathrm{Cu}\ 2p}|t|\phi_m\rangle \times \langle \phi_{\mathrm{Cu}\ 2p}|t|\phi_n\rangle|^2 \int \frac{\rho_m(\varepsilon)\rho_n'(\varepsilon+\Omega-\omega)}{(\varepsilon-\varepsilon_{\mathrm{Cu}\ 2p}-\omega)^2+\Gamma^2} d\varepsilon, \quad (1)$$

where *t* is a dipole operator acting between Cu 2*p* core states

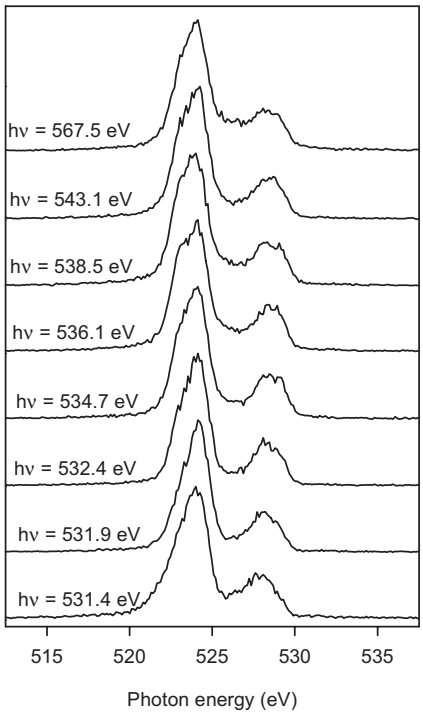

FIG. 6. O K x-ray emission spectra of Cu_2O excited over a range of photon energies close to threshold. The emission features show little change with changing photon energy.

and valence and conduction band states ϕ_m and ϕ_n of appropriate symmetry and Γ represents the broadening due to the core hole. Since both Cu $2p$ to Cu $3d$ and Cu $2p$ to Cu $4s$ matrix elements are nonzero, the summation should include the four possible convolutions between the occupied and empty Cu $3d$ and $4s$ partial densities of states corresponding to the allowed channels in electronic Raman scattering where $\Delta l=0$ or $\Delta l=\pm 2$, i.e., the summation should include the integrals involving $\rho_{\mathrm{Cu}\ 3d}\rho'_{\mathrm{Cu}\ 3d}$, $\rho_{\mathrm{Cu}\ 3d}\rho'_{\mathrm{Cu}4s}$, $\rho_{4s}\rho'_{\mathrm{Cu}\ 3d}$, and $\rho_{\mathrm{Cu}\ 4s}\rho'_{\mathrm{Cu}\ 4s}$. We have evaluated the four energy-weighted convolutions given in expression (1) and these are shown in Fig. 8. Finally, we computed a theoretical RIXS by weighting squares of matrix elements involving Cu $4s$ states by a factor of $1/10$ as compared to those involving Cu $3d$ states. The results of this computation are also shown in Fig. 8 along with an experimental loss spectrum. Although the basic shape of the computed spectral profile is similar to that observed experimentally, the maximum in the experimental spectrum is about almost 2 eV lower in energy than calculated. This is despite the agreement between experimental and theoretical band gaps. We attribute this discrepancy to excitonic effects. In fact, the shift in the emission spectrum is very close to the shift in the absorption spectrum associated with the core-hole potential. This observation has prompted us to adopt an *ad hoc* procedure for calculation of the inelastic loss spectrum in which the empty density of states from the band structure calculation in Eq. (1) is replaced by what we might call an excitonic density of states derived from experimental x-ray absorption spectrum. As shown in Fig. 8 with this approach, there is better agreement between observed and calculated spectra. Proper justification of the procedure is, however, problematic: the excitonic nature of the L shell x-ray absorption spectrum depends on the presence of the Cu $2p$ core hole, but in the RIXS final state, there is obviously no core hole. In general, RIXS spectra have, in the past, been found to be relatively insensitive to core-hole ef-

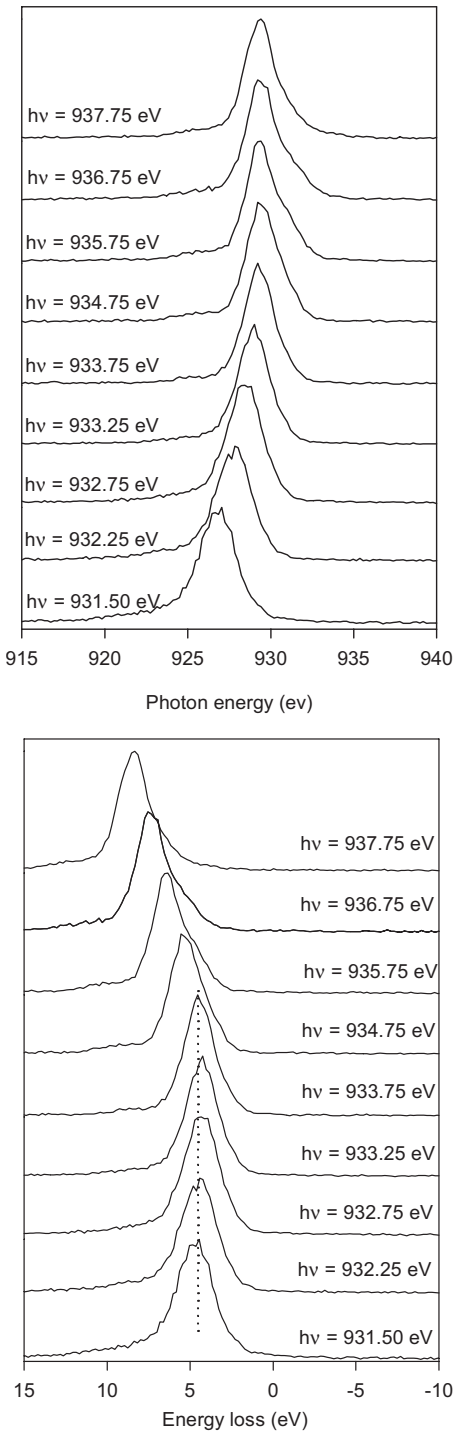

FIG. 7. Upper panel: Cu L_3 x-ray emission spectra of Cu_2O excited over a range of photon energies close to the threshold. The emission features show strong variation in energy for exciting photon energies closest to the thresholds between 931.50 and 934.75 eV. Lower panel: emission spectra as above but presented on an energy loss scale.

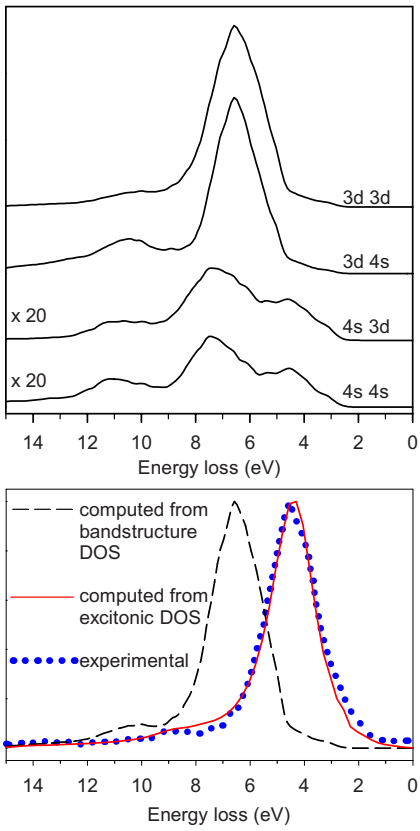

FIG. 8. (Color online) Upper panel. Computed terms for the four dipole allowed channels included in the summation in Eq. (1). Lower panel. Dashed line: computed inelastic x-ray scattering spectrum, which is obtained by appropriately weighting the four channels shown above. Solid line: computed inelastic scattering spectrum using "excitonic" density of states. In all cases, the simulated spectra have been broadened by a Gaussian with full width at half maximum height of 1.35 eV to include the effects of broadening of the core hole. Dotted line: experimental energy loss spectrum excited at $h\nu$=933.75 eV.

fects for simple materials such as graphite and *c*- and *h*-BN, where the main effect is to produce a redistribution of spectral weight.[57–61] On the other hand, electron-valence hole interactions in the final state are known to enhance spectral weight at higher emission energies, i.e., at lower loss energies, as is observed here. The valence electron exciton binding energy in Cu_2O is only about 0.14 eV.[62,63] However, the influence of final state exciton binding on the RIXS spectra may be amplified by localization of the conduction band electron by the core hole in the intermediate state.[55] A fuller treatment of this problem will be presented elsewhere.

It is finally interesting to note that the lowest photon energy for which there is no longer evidence of loss structure is 934.75 eV, which is sufficient to promote an L_3 electron into the conduction band. In other words, the range of photon energies under which inelastic x-ray scattering is observed is all in the excitonic regime, as shown schematically in Fig. 5. It is also significant that O *K* excitation does not give a true core exciton and that no energy loss structure can be identified at the O *K* edge.

V. CONCLUDING REMARKS

First principles calculations on Cu_2O using a hybrid exchange approximation to density functional theory show that there is pronounced mixing between Cu 3*d* and O 2*p* states and that along with strong on-site hybridization between Cu $3d_{z^2}$ and Cu 4*s* states, this mixing introduces significant Cu 3*d* character into the conduction band of this oxide. Valence level photoemission spectroscopy in combination with O *K* shell and Cu *L* shell x-ray emission spectra confirms that there is indeed pronounced cation-anion hybridization.

Well-defined features are observed at a loss energy of 4.5 eV in resonant inelastic scattering close to the Cu 2*p* core threshold. To date, most previous experimental works on resonant inelastic x-ray scattering of Cu compounds at the *L* edge have concentrated on open shell Cu(II) species,[64] including CuO (Ref. 65) and layered cuprates such as La_2CuO_4,[65–67], $Sr_2CuO_2Cl_2$,[67] $Bi_2Sr_2CaCu_2O_{8+\delta}$,[67] and $Tl_2Ba_2CaCu_2O_8$.[68] Here, the loss structure is typically found between 1.5 and 2.0 eV to low energy of the incident photon energy and can be understood in terms of localized excitations within the 3*d* manifold of energy levels, which are split by the ligand field.[61,67] The excitations found in the present work are at much higher loss energy and cannot be associated with ligand field excitations in the conventional sense because Cu_2O is a closed shell material. In the ionic limit, the interband excitations we have observed could be described as 3*d* to 4*s* transitions. However, on-site Cu $3d_{z^2}$–Cu 4*s* hybridization introduces significant Cu 3*d* character into the conduction band and the much bigger dipole matrix elements between core Cu 2*p* states and Cu 3*d* states as compared to Cu 2*p* to Cu 4*s* matrix elements means that the observed inelastic scattering is dominated by a convolution between the full and empty Cu 3*d* partial density of states. Similar structure to that found here for Cu_2O has been observed in RIX spectra of $CuAlO_2$ (Ref. 69) where a pronounced energy loss feature is found at 5.4 eV for excitation energies close to the L_3 core threshold. $CuAlO_2$ is another Cu(I) compound with linear coordination of Cu by two oxygen nearest neighbors. The similarity between the loss spectra of the two materials suggests that on-site interband excitations may be a general feature of RIX spectra of Cu(I) $3d^{10}$ materials.

ACKNOWLEDGMENTS

Computer resources on the HPCx service were provided via our membership of the UK's HPC Materials Chemistry Consortium and funded by EPSRC (Portfolio Grant No. EP/D504872). Experimental work on transparent conducting oxides in Oxford is supported by EPSRC under Grant No. GR/S94148 and the NCESS Facility by Grant Scienta XPS facility by EPSRC under Grant No. EP/E025722/1. The Boston University program is supported in part by the U.S.

Department of Energy under No. DE-FG02-98ER45680 and in part by the Donors of the American Chemical Society Petroleum Research Fund. The Advanced Light Source is supported by the Director, Office of Science, Office of Basic Energy Sciences, U.S. Department of Energy under Contract No. DE-AC02-05CH11231.

*Corresponding author. russell.egdell@chem.ox.ac.uk

[1] For example, for a discussion of *n*-type doping in In_2O_3, see, C. G. Granqvist and A. Hultåker, Thin Solid Films **411**, 1 (2002).
[2] T. Yamamoto and H. K. Yoshida, Jpn. J. Appl. Phys., Part 2 **38**, L166 (1999).
[3] M. Joseph, H. Tabata, and T. Kawai, Jpn. J. Appl. Phys., Part 2 **38**, L1205 (1999).
[4] A. Tsukazaki, A. Ohtomo, T. Onuma, M. Ohtani, T. Makino, M. Sumiya, K. Ohtani, S. F. Chichibu, S. Fuke, Y. Segawa, H. Ohno, H. Koinuma, and M. Kawasaki, Nat. Mater. **4**, 42 (2005).
[5] S. Nikitine, J. B. Grun, and M. Sieskind, J. Phys. Chem. Solids **17**, 292 (1961).
[6] H. Kawazoe, M. Yasukawa, H. Hyodo, M. Kurita, H. M. Yanagi, and H. Hosono, Nature (London) **389**, 939 (1997).
[7] H. Yanagi, S. Inoue, K. Ueda, H. Kawazoe, H. Hosono, and N. Hamada, J. Appl. Phys. **88**, 4159 (2000).
[8] K. Ueda, T. Hase, H. Yanagi, H. Kawazoe, H. Hosono, H. Ohta, M. Orita, and M. Hirano, J. Appl. Phys. **89**, 1790 (2001).
[9] H. Yanagi, H. Kawazoe, A. Kudo, M. Yasukawa, and H. Hosono, J. Electroceram. **4**, 407 (2000).
[10] H. Yanagi, T. Hase, S. Ibuki, K. Ueda, and H. Hosono, Appl. Phys. Lett. **78**, 1583 (2001).
[11] X. L. Nie, S. H. Wei, and S. B. Zhang, Phys. Rev. Lett. **88**, 066405 (2002).
[12] A. Kudo, H. Yanagi, H. Hosono, and H. Kawazoe, Appl. Phys. Lett. **73**, 220 (1998).
[13] H. Ohta, M. Orita, M. Hirano, I. Yagi, K. Ueda, and H. Hosono, J. Appl. Phys. **91**, 3074 (2002).
[14] S. N. Kale, S. B. Ogale, S. R. Shinde, M. Sahasrabuddhe, V. N. Kulkarni, R. L. Greene, and T. Venkatesan, Appl. Phys. Lett. **82**, 2100 (2003).
[15] M. Ivill, M. E. Overberg, C. R. Abernathy, D. P. Norton, A. F. Hebard, N. Theodoropoulou, and J. D. Budai, Solid-State Electron. **47**, 2215 (2003).
[16] M. Wei, N. Braddon, D. Zhi, P. A. Midgley, S. K. Chen, M. G. Blamire, and J. L. MacManus-Driscoll, Appl. Phys. Lett. **86**, 072514 (2005).
[17] L. Q. Pan, H. Zhu, C. F. Fan, W. G. Wang, Y. Zhang, and J. Q. Xiao, J. Appl. Phys. **97**, 10D318 (2005).
[18] J. Drahokoupil, M. Polcik, and E. Pollert, Solid State Commun. **66**, 4 (1988).
[19] J. Drahokoupil, M. Polcik, and E. Pollert, Solid State Commun. **74**, 8 (1990).
[20] D. R. Mueller, J. Wallace, D. L. Ederer, J. J. Jia, W. L. O'Brien, Q. Y. Dong, and T. A. Callcott, Phys. Rev. B **46**, 11069 (1992).
[21] J. M. Mariot, V. Branole, C. F. Hague, G. Vetter, and F. Queyroux, Z. Phys. B: Condens. Matter **75**, 1 (1989).
[22] G. K. Wertheim and S. Hüfner, Phys. Rev. Lett. **28**, 1028 (1972).
[23] J. Ghijsen, L. H. Tjeng, J. vanElp, H. Eskes, J. Westerink, G. A. Sawatzky, and M. T. Czyzyk, Phys. Rev. B **38**, 11322 (1988).
[24] S. L. Hulbert, B. A. Bunker, F. C. Brown, and P. Pianetta, Phys. Rev. B **30**, 2120 (1984).
[25] M. Grioni, J. F. van Acker, M. T. Czyzyk, and J. C. Fuggle, Phys. Rev. B **45**, 3309 (1992).
[26] M. Grioni, J. B. Goedkoop, R. Schoorl, F. M. F. deGroot, J. C. Fuggle, F. Schafers, E. E. Koch, G. Rossi, J. M. Esteva, and R. C. Karnatak, Phys. Rev. B **39**, 1541 (1989).
[27] A. F. Wells, *Structural Inorganic Chemistry* (Clarendon, Oxford, 1984).
[28] R. Mittal, S. L. Chaplot, S. K. Mishra, and P. P. Bose, Phys. Rev. B **75**, 174303 (2007).
[29] U. Fano and J. W. Cooper, Rev. Mod. Phys. **40**, 441 (1968).
[30] R. Dovesi, V. R. Saunders, C. Roetti, R. Orlando, C. M. Zicovich-Wilson, F. Pascale, B. Civalleri, K. Doll, N. M. Harrison, I. J. Bush, Ph. D'Arco, and M. Llunell, *CRYSTAL06 User'sManual* (University of Torino, Torino, 2006).
[31] X.-B. Feng and N. M. Harrison, Phys. Rev. B **69**, 132502 (2004).
[32] J. Muscat, A. Wander, and N. M. Harrison, Chem. Phys. Lett. **342**, 397 (2001).
[33] K. Doll and N. M. Harrison, Chem. Phys. Lett. **317**, 282 (2000).
[34] M. I. McCarthy and N. M. Harrison, Phys. Rev. B **49**, 8574 (1994).
[35] K. H. Schulz and D. F. Cox, Phys. Rev. B **43**, 1610 (1991).
[36] D. F. Cox and K. H. Schulz, Surf. Sci. **249**, 138 (1991).
[37] D. F. Cox and K. H. Schulz, Surf. Sci. **256**, 67 (1991).
[38] *Practical Surface Analysis*, edited by D. Briggs and M. P. Seah (Wiley, Chichester, 1990).
[39] J. Nordgren and R. Nyholm, Nucl. Instrum. Methods Phys. Res. A **246**, 242 (1986).
[40] J. Nordgren, G. Bray, S. Cramm, R. Nyholm, J. E. Rubensson, and N. Wassdahl, Rev. Sci. Instrum. **60**, 1690 (1989).
[41] J. P. Dahl and A. C. Switendick, J. Phys. Chem. Solids **27**, 931 (1966).
[42] L. Kleinman and K. Mednick, Phys. Rev. B **21**, 1549 (1980).
[43] J. Robertson, Phys. Rev. B **28**, 3378 (1983).
[44] P. Marksteiner, P. Blaha, and K. Schwarz, Z. Phys. B: Condens. Matter **64**, 119 (1986).
[45] E. Ruiz, S. Alvarez, P. Alemany, and R. A. Evarestov, Phys. Rev. B **56**, 7189 (1997).
[46] A. Martinez-Ruiz, M. G. Moreno, and N. Takeuchi, Solid State Sci. **5**, 291 (2003).
[47] X. Nie, S.-H. Wei, and S. B. Zhang, Phys. Rev. B **65**, 075111 (2002).
[48] A. Filippetti and V. Fiorentini, Phys. Rev. B **72**, 035128 (2005).
[49] M. Nolan and S. D. Elliot, Phys. Chem. Chem. Phys. **8**, 5350 (2006).
[50] Y. Dou, R. G. Egdell, D. S. L. Law, N. M. Harrison, and B. G. Searle, J. Phys.: Condens. Matter **10**, 8447 (1998).
[51] L. E. Orgel, J. Chem. Soc. 4186 (1958).
[52] A. Önsten, M. Mansson, T. Claesson, T. Muro, T. Matsushita, T. Nakamura, T. Kinoshita, U. O. Karlsson, and O. Tjernberg, Phys. Rev. B **76**, 115127 (2007).
[53] J. P. Hu, D. J. Payne, R. G. Egdell, N. M. Harrison, and V. R.

Dhanak, Chem. Phys. Lett. **450**, 39 (2007).
[54] J. J. Yeh and I. Lindau, At. Data Nucl. Data Tables **32**, 1 (1985).
[55] A. Kotani and S. Shin, Rev. Mod. Phys. **73**, 203 (2001).
[56] J. Jiménez-Mier, J. van Ek, D. L. Ederer, T. A. Callcott, J. J. Jia, J. Carlisle, L. Terminello, A. Asfaw, and R. C. Perera, Phys. Rev. B **59**, 2649 (1999).
[57] E. L. Shirley, Phys. Rev. Lett. **80**, 794 (1998).
[58] E. L. Shirley, J. A. Soininen, G. P. Zhang, J. A. Carlisle, T. A. Callcott, D. L. Ederer, L. J. Terminello, and R. C. Perera, J. Electron Spectrosc. Relat. Phenom. **114-116**, 939 (2001).
[59] T. Minami and K. Nasu, J. Electron Spectrosc. Relat. Phenom. **92**, 231 (1998).
[60] M. vanVeenendaal and P. Carra, Phys. Rev. Lett. **78**, 2839 (1997).
[61] T. Minami, J. Phys. Soc. Jpn. **67**, 3598 (1998).
[62] V. T. Agekyan, Phys. Status Solidi A **43**, 11 (1977).
[63] D. P. Trauernicht, J. P. Wolfe, and A. Mysyrowicz, Phys. Rev. Lett. **52**, 855 (1984).
[64] S. Tanaka and A. Kotani, J. Phys. Soc. Jpn. **62**, 464 (1993).
[65] K. Ichikawa, K. Jouda, S. Tanaka, K. Soda, M. Matsumoto, Y. Taguchi, T. Katsumi, O. Aita, H. Maezawa, Y. Azuma, and H. Kitzawa, J. Electron Spectrosc. Relat. Phenom. **78**, 183 (1996).
[66] L. C. Duda, G. Dräger, S. Tanaka, A. Kotani, J. Guo, D. Heumann, S. Bocharov, N. Wassdahl, and J. Nordgren, J. Phys. Soc. Jpn. **67**, 416 (1998).
[67] G. Ghiringhelli, N. B. Brookes, E. Annese, H. Berger, C. Dallera, M. Grioni, L. Perfetti, A. Tagliaferri, and L. Braicovich, Phys. Rev. Lett. **92**, 117406 (2004).
[68] W. A. Little, M. J. Holcomb, G. Ghiringhelli, L. Braicovich, C. Dallera, A. Piazzalunga, A. Tagliaferri, and N. B. Brookes, Physica C **460-462**, 40 (2007).
[69] D. J. Aston, D. J. Payne, A. J. H. Green, R. G. Egdell, D. S. L. Law, J. Guo, P. A. Glans, T. Learmonth, and K. E. Smith, Phys. Rev. B **72**, 195115 (2005).